Varicose instabilities in turbulent boundary layers

Skote, M.; Haritonidis, J. H.; Henningson, D. S.

2002

Skote, M., Haritonidis, J. H., & Henningson, D. S. (2002). Varicose instabilities in turbulent boundary layers. Physics of fluids, 14(7), 2309-2323.

https://hdl.handle.net/10356/101661

https://doi.org/10.1063/1.1482377

Varicose instabilities in turbulent boundary layers

M. Skote
Department of Mechanics, Royal Institute of Technology (KTH), SE-100 44 Stockholm, Sweden

J. H. Haritonidis
Department of Aerospace Engineering and Aviation, Ohio State University, Columbus, Ohio 43210

D. S. Henningson
Department of Mechanics, Royal Institute of Technology (KTH), SE-100 44 Stockholm, Sweden

(Received 7 November 2001; accepted 10 April 2002; published 31 May 2002)

An investigation of a model of turbulence generation in the wall region of a turbulent boundary layer is made through direct numerical simulations. The model is based on the varicose instability of a streak. First, a laminar boundary layer disturbed by a continuous blowing through a slot is simulated in order to reproduce and further investigate the results reported from the experiments of Acarlar and Smith [J. Fluid Mech. **175**, 43 (1987)]. An isolated streak with an inflectional profile is generated that becomes unstable, resulting in a train of horseshoe vortices. The frequency of the vortex generation is equal to the experimental results. Comparison of the instability characteristics to those predicted through an Orr–Sommerfeld analysis are in good agreement. Second, a direct numerical simulation of a turbulent boundary layer is performed to point out the similarities between the horseshoe vortices in a turbulent and a laminar boundary layer. The characteristics of streaks and the vortical structures surrounding them in a turbulent boundary layer compare well with the model streak. The results of the present study show that one mechanism for the generation of horseshoe vortices in turbulent boundary layers is related to a normal inflectional instability of the streaks. © *2002 American Institute of Physics.* [DOI: 10.1063/1.1482377]

I. INTRODUCTION

A. Detection of coherent structures

The occurrence of coherent vortices in wall-bounded turbulent flows has been observed in a large number of investigations by different means. The experimental observations have relied on dye injections or hydrogen bubbles introduced in the flow. Lately, low Reynolds number flows have been investigated numerically through direct numerical simulations (DNS). The flow field variables are all available at the same time and thus more sophisticated detection methods have been developed. Robinson[1] used the pressure successfully for revealing horseshoe vortices in a data base from a DNS of a turbulent boundary layer. Singer and Joslin[2] also used the pressure in a numerical simulation for visualizing a horseshoe vortex generated by blowing through a slot. Chong *et al.*[3] used the discriminant of the velocity gradient tensor for identifying flow structures in turbulent boundary layers. They found structures that to a great extent consist of attached vortex loops. Zhou *et al.*[4] used the imaginary part of the complex eigenvalue of the velocity gradient tensor to identify hairpin structures in channel flow. The structures originated from a vortical structure imposed in the flow. By plotting the imaginary part a clear picture of the structure was obtained and the shape was not sensitive to the level chosen for visualization. Jeong and Hussain[5] and Schoppa and Hussain[6] used an eigenvalue based on the Hessian of the pressure for identification of vortices in a turbulent channel flow, and used conditional sampling to extract the precise form of the coherent structure.

B. Streamwise versus horseshoe vortex structures

Jeong and Hussain[5] did not detect any horseshoe vortices in the channel flow simulation by Kim *et al.*[7] Instead they extracted a coherent structure consisting of quasi-streamwise vortices by conditional sampling. Jimenez and Moin[8] and Hamilton *et al.*[9] observed, by shrinking the computational box, that the self-sustained turbulence is linked to the quasi-streamwise vortices, and does not depend on the outer part of the flow. This scenario is consistent with the model of Waleffe[10] which states that the vortex is fed by energy from the break up of the streak. Jimenez and Pinelli[11] used a method of reducing the influence of the outer flow in a numerical simulation to show that the regeneration cycle is independent on the outer flow. Thus, according to these findings, there is little interaction between the inner and outer flow. Consequently, it is possible to model the regeneration of turbulence via a self-sustaining process involving low-speed streak and quasi-streamwise vortex, independent on the outer flow.

On the other hand, horseshoe vortices observed in boundary layer flows reach into the outer flow. Experimental evidence include the work of Acarlar and Smith[12] and Haidari and Smith[13] in which vortices, generated by blowing fluid through a slot in the wall, were studied in a laminar bound-

ary layer. The blowing was continuous in the experiment by Acarlar and Smith while a pulsed injection was used by Haidari and Smith. Recently, Adrian *et al.*[14] have visualized hairpin vortices in a turbulent boundary layer using particle image velocimetry (PIV). They show that hairpin packets (groups of horseshoe vortices) build up the turbulent boundary layer. The number of vortices that constitute a packet is lower in a low Reynolds number flow than in high Reynolds number flows. Further experiments with conditional sampling by Christensen and Adrian[15] revealed that the outer structure of the turbulent boundary layer includes spanwise vortices at a spacing and angle which are Reynolds number independent.

The experimental findings of Haidari and Smith was confirmed by the DNS of Singer and Joslin.[2] They observed different kinds of subsidiary vortices (such as necklace or U-shaped vortices) and the initial vortex generated by the blowing finally develops into a turbulent spot.

The size of the horseshoe vortices seems to vary within the flow and also vary with Reynolds number. A turbulence model for Reynolds average Navier–Stokes (RANS) calculations of turbulent flows has been developed by Perry *et al.*[16] based on size and strength of the horseshoe structures. This technique was recently used by Marusic[17] to show that packets of horseshoe vortices are statistically significant structures.

C. Streak instability and turbulence regeneration

The vortex structures present in turbulent boundary layers seem to be related to streak instabilities. However, several types of instabilities seem to occur. Robinson[18] proposed that a normal inflectional instability of the instantaneous velocity profile may produce horseshoe vortices. Singer[19] showed that a normal inflectional instability of the velocity profile may be responsible for the generation of secondary horseshoe vortices. Kim *et al.*[20] were the first to show that a normal inflectional instability of the instantaneous velocity profile is of importance in the turbulence regeneration cycle. They observed the inflectional velocity profiles in connection with the rapid lift up of the low-speed streaks in the later part of the process of the streak break up. Several models of the turbulence regeneration cycle have been proposed by Landahl,[21,22] where inflectional instability of the local mean velocity profile is a main ingredient.

On the other hand, in the model of Waleffe[10] the basic state is two-dimensional and consists of the turbulent mean flow with a simple construction of the streak imposed. He found that the dominating instability is sinuous and that it is correlated with the spanwise inflection of the basic state. Kawahara *et al.*[23] and Schoppa and Hussain[6] also used such a model and showed that the varicose mode is stable. Schoppa and Hussain[6] argued that this is consistent with the absence of horseshoe vortices in their examination of the DNS data base generated by Kim *et al.*[7]

The references cited above form only a small part of the work that has been put into the detection and analysis of coherent structures. A recent article by Schoppa and Hussain,[24] where a detailed discussion of the state of the art is included, categorizes the mechanisms into parent-offspring and instability based scenarios. The former is characterized as the generation of vortices by direct action of existing vortices, whereas the second involves local instability of quasi-steady flow. Within the instability based scenarios the sinuous and varicose streak instabilities are the two main ones. The view of Schoppa and Hussain[24] seems to be that there is a contradiction between these explanations. Our view is that turbulence is such a rich phenomenon that there are most likely several mechanisms at work regarding coherent structure generation, of which we here have chosen to study one.

D. Present study

In this work we will pursue the horseshoe vortex dynamics, within the streak stability based scenario of varicose type. In the experiments by Acarlar and Smith,[12] hereafter denoted AS, an artificial low-speed streak was generated in a laminar boundary layer by blowing fluid through a slot in the wall. The streak became unstable and horseshoe vortices were formed and were followed downstream. In the present study we reproduce the flow studied by AS through DNS. Moreover, the hypothesis indicated by AS regarding the instability causing the vortices is here further investigated. One of the objectives in the AS experiment was to give insight to the mechanisms and structures in a turbulent boundary layer. In the present work, a stronger link to turbulence is made through comparison with a simulation of a zero pressure gradient turbulent boundary layer.

The experiments by Haidari and Smith[13] could also have been reproduced with our numerical code by turning off the blowing after the injection was completed. However, the numerical study by Singer and Joslin[2] was already performed as a numerical compliment to the pulsed injection experiments by Haidari and Smith. Note also that although the pulsed injection is important for the study of a single vortex developing downstream, the turbulent boundary layer seems mostly to consist of packages of vortices, see, e.g., Adrian *et al.*[14]

After a presentation of the numerical method and parameters in Sec. II, we present the results in Sec. III. The emphasis is on the results from the laminar simulation, which is compared with the experimental results from AS. Further investigations of the instability mechanism are made. Also comparison with the turbulent simulation is done, from which strong similarities between the two cases are presented.

II. NUMERICAL METHODOLOGY

A. Direct numerical simulations

The code used for the simulation is developed at KTH and FFA.[25] The program uses spectral methods with Fourier discretization in the horizontal directions and Chebyshev discretization in the normal direction. Since the boundary layer is developing in the down-stream direction, it is necessary to use nonperiodic boundary conditions in the streamwise direction. This is possible while retaining the Fourier discretization if a fringe region is added downstream of the physical

domain. In the fringe region the flow is forced from the outflow of the physical domain to the inflow. In this way the physical domain and the fringe region together satisfy periodic boundary conditions. The fringe region is implemented by the addition of a volume force whose form is designed to minimize the upstream influence. The upstream influence of the fringe region is of the same order as the height of the computational box. Since our box is very long and thin, the influence is marginal. All the results are taken from regions well upstream of any fringe influence. For an analysis of the fringe region technique, the reader is referred to the investigation by Nordström *et al.*[26]

Time integration is performed using a third order Runge–Kutta scheme for the advective and forcing terms and Crank–Nicholson for the viscous terms.

All quantities are nondimensionalized by the freestream velocity (U_∞) and the displacement thickness (δ^*) at the starting position of the simulation ($x=0$) where the flow is laminar. At that position $Re_{\delta^*}=U_\infty\delta^*/\nu=450$ for all simulations, except for some simulations performed at $Re_{\delta^*}=290$ for the comparison of frequency characteristics. The length (including the fringe), height and width of the computation box were $260\times7\times14$ in these units. The number of modes was $432\times65\times72$. The size and resolution were checked to be sufficient for all cases.

The simulations were performed with an initial objective of reproducing some of the results obtained in the experiments of AS. In their experiments the slot was 63.5 mm in length and 1 mm in width. The simulations were performed with a slot with the same length but twice the width, i.e., 2 mm. This change in geometry results in a large decrease in computational cost. The slot in simulation coordinates (δ^*) is approximately 30 long and 1 wide. The flow through the slot is set by a velocity profile resembling a channel flow parabola in the spanwise direction and is increasing from zero to the maximum value during the first 10% of the slot length at the upstream end, and is likewise terminated at the downstream end. The blowing through the slot was continued without interruption through all of the simulations. To avoid large transients in the beginning of the simulation we ramped up the blowing from zero to the maximum value during an initial time of $10(\delta^*/U_\infty)$. The time step was considerably decreased when the blowing through the wall is applied. The strength of the blowing was varied from 6.5% to 20% of the freestream velocity.

A low-speed streak is formed immediately above the slot due to the lift-up of low-speed fluid to the flow further out in the boundary layer. A disturbance on this streak was detected and the frequency was observed during a long period of time, and was then locked by letting a small (1% of the original blowing) additional time-periodic blowing be superimposed on the blowing forming the streak. The frequency of the initial disturbance on the streak was locked to be able to calculate the growth rate of the disturbance through a Fourier transform in time.

A simulation of a turbulent boundary layer was performed to investigate how the streak instabilities observed in the isolated streak in the laminar boundary layer could be applicable to a turbulent flow. The same code was used, but the laminar boundary layer was disturbed at the beginning of the computational box by a random volume force near the wall. The length (including the fringe), height and width of the computation box were $600\times30\times34$. The number of modes was $640\times201\times128$. The simulations were performed at $Re_{\delta^*}=450$ for the laminar inflow before the tripping, which gives a turbulent Re_Θ: 343–636. The resolution in plus units was $\Delta X^+=19$, $\Delta Z^+=5.5$, and ranging from $\Delta Y^+=0.04$ close to the wall to $\Delta Y^+=5.6$ at the coarsest part of the grid.

B. The linear stability analysis

One of the main conclusions of this work will concern the instability mechanism of a low-speed streak leading to horseshoe-shaped vortices. Linear stability theory will be used to describe the early stages of this instability. The disturbance occurring due to the instability of the streak will be denoted secondary disturbance, since the primary disturbance is the streak itself. The velocity profiles close to where the secondary disturbance start to appear, below denoted $U=U(y)$, were analyzed by solving the Orr–Sommerfeld (OS) equation. The results from the OS equation are only relevant as long as the disturbance is small enough and variations of the base flow (streak) in the horizontal directions and time is much smaller than the length scale of the instability waves. The OS equation is the linearized Navier–Stokes equations for the disturbance,

$$\phi''''-2\alpha^2\phi''+\alpha^4\phi=i\alpha R[(U-c)(\phi''-\alpha^2\phi)-U''\phi]. \quad (1)$$

The two-dimensional disturbance is written as a stream function

$$\psi=\phi(y)\exp[i\alpha(x-ct)]=\phi(y)\exp[i(\alpha x-\omega t)]. \quad (2)$$

Because the secondary disturbance is characterized by its frequency and its growth in space in the simulations, spatial analysis of the OS equation will be used. In the case of spatial analysis the eigenvalue problem (1) is solved for a given R and ω, which is real. The solution is $\phi(y)$ (eigenfunction) and $\alpha=\alpha_r+i\alpha_i$ (eigenvalue). The value of $-\alpha_i$ is the growth rate, and α_r is the streamwise wave number.

The results from the analysis of the OS equation are compared with the actual behavior of the flow in the DNS. The eigenvalue $-\alpha_i$ is compared with the growth rate of the disturbance. Furthermore, the eigenvalue α_r is compared with the streamwise wave number of the disturbance. The analysis of the time signal from DNS is done through a Fourier transform in time of the velocity fields. For a given frequency, we take the maximum over the spanwise and normal directions. Thus, the results from DNS are contained in a function $\hat{u}(x)$. The growth rate of the disturbance is

$$\sigma=-Re\left\{\frac{1}{\hat{u}}\frac{d}{dx}\hat{u}\right\}, \quad (3)$$

and the streamwise wave number of the disturbance is

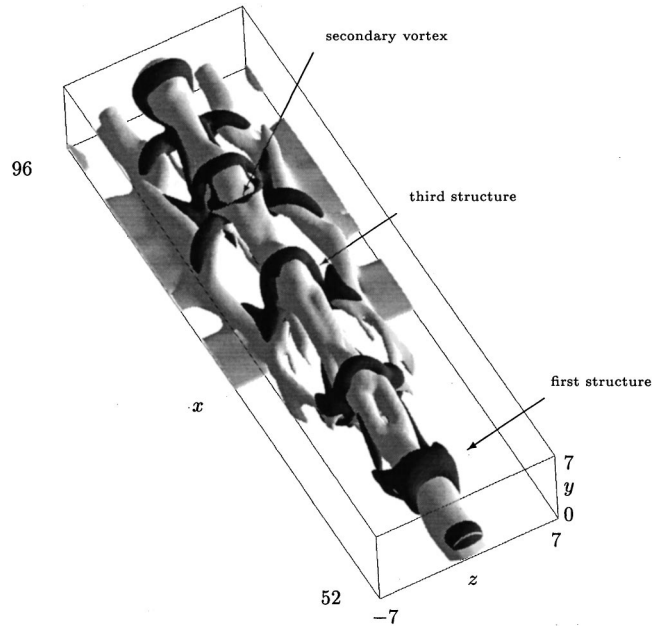

FIG. 1. The flow field downstream of the slot. The light gray structures represent the low-speed streaks and the darker ones represent regions with low pressure. Contour levels are -0.08 for the streamwise velocity fluctuations and -0.01 for the pressure.

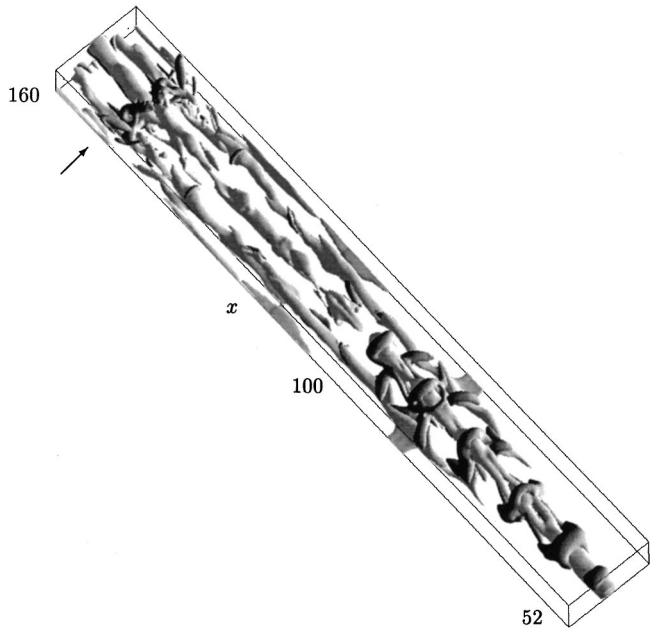

FIG. 2. The flow field far downstream of the slot. The light gray structures represent the low-speed streaks and the darker ones represent regions with low pressure. Contour levels are -0.11 for the streamwise velocity fluctuations and -0.005 for the pressure.

$$\tilde{\alpha} = Im\left\{\frac{1}{\hat{u}}\frac{d}{dx}\hat{u}\right\}. \tag{4}$$

The use of the Orr–Sommerfeld equation proposed here does not take the spanwise variation of the streak profile into account. Although this could in principle be done, it would defeat our purpose which is to show that an instability due to the normal shear is the dominating growth mechanism responsible for the initiation of the horseshoe vortex. We are interested in obtaining a simple model which we can apply in the more complicated turbulent case, in the same manner as Waleffe[10] models the sinuous secondary instability of a turbulent streak with only a spanwise varying shear. In addition, a 2D stability analysis would also be superfluous since we extract a result equivalent to such an analysis from the DNS calculations. In fact, the DNS results can be considered as a secondary instability calculation, where not only the spanwise shear is taken into account, but also the streamwise nonparallel effects, as long as the amplitude of the disturbance is small.

III. RESULTS

A. Initial observations

1. Comparison with AS experiment

The development of the streak downstream of the slot is shown in Fig. 1. Only the part immediately after the slot is shown. The light gray iso-surface represents the low-speed streak, and the dark gray represents the low pressure. The slot ends at $x=60$ and the first low-pressure structure is observed at that point. The subsequent pressure structures develop downstream and become stronger. Additional streaks on either side are being induced by the pressure structure at $x=70$. This will be further discussed in Sec. III B. Around $x=94$ the last structure in the train of vortices is observed, and the streak has been lifted upward. The low-pressure structure vanishes, but the streak and the additional, induced streaks persist downstream, as seen from Fig. 2, where the region downstream of the breakup is also shown. The three

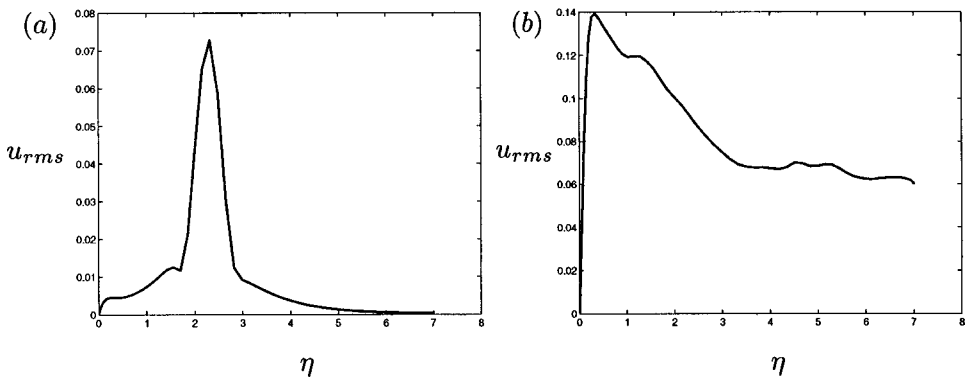

FIG. 3. u_{rms} at (a) $x=60$, (b) $x=160$.

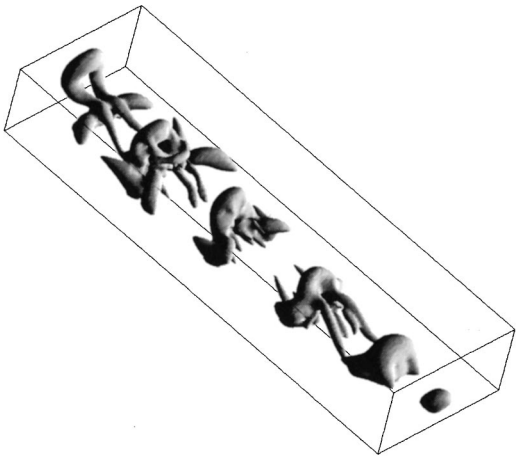

FIG. 4. Iso-surface of low pressure just downstream of the slot. Same part of the flow field as in Fig. 1.

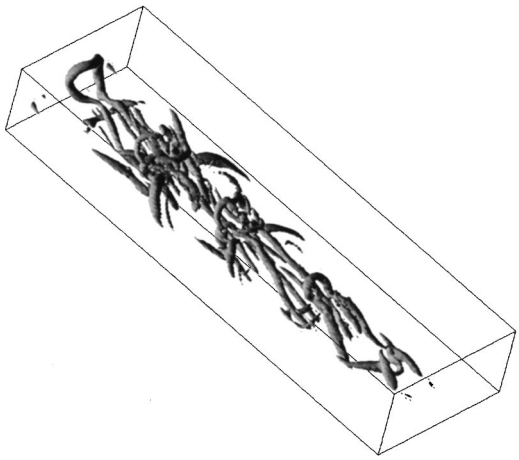

FIG. 5. Iso-surface of the imaginary part of the eigenvalue of velocity gradient tensor. The figure shows the eigenvalue calculated from the same velocity field as in Fig. 4. Contour level at 0.32.

streaks continue far downstream until more complicated low-pressure structures occur at $x=145$, marked with an arrow in Fig. 2. Here the flow has more of a turbulent nature, which is also seen from the rms-values shown in Fig. 3. The u_{rms} profile from a position at the end of the slot is shown in Fig. 3(a). This profile has a shape which is a result of an inflectional instability, which will be further discussed in Sec. III D. The u_{rms} from a position far downstream ($x=160$) is shown in Fig. 3(b). This profile resembles a profile from a turbulent boundary layer. Thus, the more turbulent like flow at the far downstream region is revealed both in the structures themselves and in the statistical profiles. The streak spacing is actually 100 in viscous units in this region, further indicating attributes of a turbulent boundary layer.

In AS no spreading of the structures were observed and they argue that this is due to the sub-critical laminar boundary layer in their experiment. They do however observe a more turbulent like profile downstream and also three elongated low-speed streaks, originating from secondary streamwise vortices. Our simulation continue further downstream than the experiment by AS, and the persistent low-speed streaks were observed downstream until the more complicated vortices appeared at $x=145$, see Fig. 2.

It was shown, in the experiments by Haidari and Smith[13] of a single vortex developing downstream, that the growth of the structure is caused by both the interaction of the primary vortex with surface fluid and inviscid deformation of the vortex lines. The latter mechanism was however not found in the numerical investigation of a single vortex by Singer and Joslin.[2] Furthermore, the numerical simulation showed that the secondary vortices formed beneath the hairpin vortex legs were closely related to the initial injection and not generated by the primary vortex. Thus, it seems difficult to obtain and observe the dynamics of a single vortex; it is strongly linked to the generation process.

The low-pressure structures seen in Fig. 1 are vortex loops, consisting of swirling flow. To illustrate that the low-pressure regions consist of rotational flow, the imaginary part of the complex eigenvalue of the velocity gradient tensor can be used.[27] Because the vorticity indicates both shear and rotation, showing vorticity can be misleading when seeking parts of the flow where rotating structures are of interest. The imaginary part of the eigenvalue on the other hand, indicates where swirling occurs.

In Fig. 4 the low-pressure structures in Fig. 1 are shown without the low-speed streak to get a clearer picture of the structures themselves. The structures in Fig. 5 consist of iso-surfaces of the imaginary part of the eigenvalue. The strong correlation indicate that the structures in Fig. 4 are due to rapid rotation of the flow in the regions of low pressure.

Observe that the Ω-shape of the last structure in Fig. 5 is reminiscent of the structure observed by Zhou *et al.*[4] Also, the kink of the legs about one-third of the length from the upstream end are present in the last structure. Note that the background flow in the present simulation is laminar whereas it consisted of a turbulent mean flow in the study of Zhou *et al.*[4] The kinked legs and the curled back head of the last structure in Fig. 5 was also observed by AS at the same downstream position.

A secondary vortex is observed above the primary horseshoe vortex in the two structures before the last one in Fig. 5. The secondary vortex is also visible in one of the corresponding pressure structures as marked in Fig. 1. The secondary vortex is visible at approximately the same position as in AS. Zhou *et al.*[4] found not only secondary horseshoe vortices developing upstream of the primary vortex, but also downstream, which was not observed in the present simulation. In the experiments of AS, a secondary vortex appears to originate from the position above the legs of primary vortex. It either grows to be an independent vortex, or agglomerates with the upstream or downstream vortex. The same behavior is observed in the present simulations.

Thus, the secondary vortices appearing upstream, above the legs, of the primary one are in common with many of the experimental and numerical investigations, while the generation of downstream secondary vortices depends on the strength and duration of blowing.

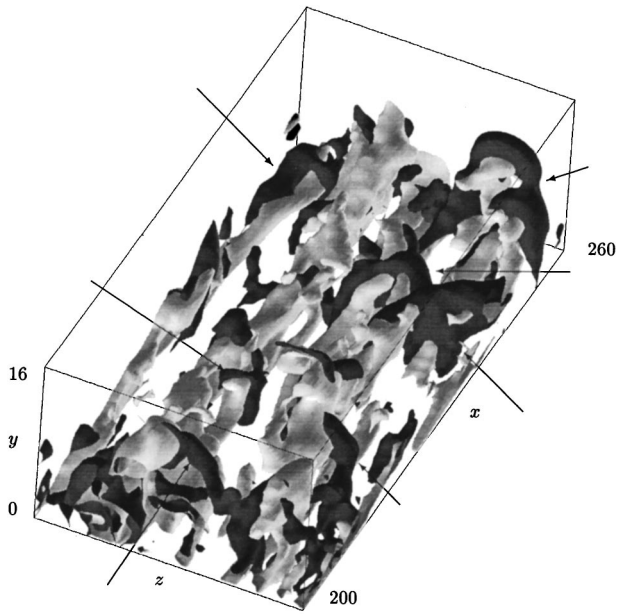

FIG. 6. Turbulent boundary layer. Only a part of the computational box is shown. The light gray structures represent the low-speed streaks and the darker ones represent regions with low pressure. Contour levels are -0.07 for the streamwise velocity fluctuations and -0.003 for the pressure. The arrows point to some typical horseshoe vortices.

2. Near-wall turbulence

The presence of streaky structures in a near-wall turbulent flow has been observed in many experiments and simulations. These structures are low speed regions, where the streamwise velocity is lower than the mean velocity, the mean taken in the spanwise (z) direction for each x- and y-position. They are narrow in the spanwise direction and elongated in the streamwise direction with a spanwise spacing of about 100 in wall units. Streaks lying at different positions in z break down at different positions in x. Also, a new streak seems to be born where the old one breaks down. In a number of investigations, events referred to as burst have been observed, and are generally considered to be part of the streak break up.

An instantaneous flow field from the simulation of a turbulent boundary layer is shown in Fig. 6. Only a part of the computational box at approximately $Re_\Theta = 450$ is shown. The spanwise width is about 300 in wall units and the height is 200. The light gray regions represent the low-speed streaks. Also shown in the figure, in the dark gray color, are regions of low pressure. The presence of horseshoe or hairpin vortices is well illustrated by this picture. The most clearly visible ones are marked with arrows in Fig. 6. It is observed that the vortices are strongly connected to the streaks, since the vortices are positioned with their head above a streak and their leg or legs on either side of the streak. This feature is common to both the laminar and turbulent streaks, cf. Figs. 1 and 6.

B. Horseshoe vortex formation

The mechanisms behind the formation of vortices from the streak is here studied in detail in the laminar flow with an artificial streak introduced. The proposed mechanism is that the low-speed streak makes the streamwise velocity profile highly inflectional. The instability is very strong (with a large growth rate). The disturbance grows downstream and higher harmonics occur. The stability analysis is presented in Sec. III D.

The results in this section are taken from the simulation at a Reynolds number $Re_{\delta^*} = U_\infty \delta^* / \nu = 450$ at $x = 0$, which corresponds to a Reynolds number $Re_{\delta^*} = 490$ at the beginning of the slot. The normal velocity blowing out of the slot was $V_w = 0.0657$, resulting in a slot Reynolds number of $Re_{V_w} = 28.3$. The blowing was introduced between $x = 30$ and $x = 59$ in the streamwise direction, and between $z = -0.48$ and $z = 0.48$ in the spanwise direction.

1. Vortex formation above the slot

One velocity field is studied, using plots in two dimensions of different planes. In Figs. 7(a)–7(f) the planes are from different positions in x, showing what happens with the flow above the slot. The lines in the horizontal direction, from blue to green, are the iso-lines of streamwise velocity, while the arrows represents the normal and spanwise velocity components. The first [Fig. 7(a)] figure shows the undisturbed laminar boundary layer at the point where the slot starts. The next one [Fig. 7(b)] shows a plane further downstream. Here the injection is visible as the strong flow out from the wall. The lines representing constant streamwise velocity are bent outward and thus forming a low-speed streak. The low-speed streak is formed because of the injection velocity that lifts up low-speed fluid from the near-wall region higher up in the laminar boundary layer. In Fig. 7(c) a swirling flow is observed at either side of the low-speed streak. As the vortical motion becomes stronger it deforms the streak as seen in Fig. 7(d), where also the vortex is strong enough to be represented with low pressure regions at the center of the vortex. Iso-lines of constant low pressure are shown as red lines. These low pressure regions that evolve from the center of the vortex at either side of the streak are the legs of the first low pressure structure seen in Fig. 1. The plane in Fig. 7(d) is located at the end of the slot, thus no more injection velocity can be observed. In Fig. 7(e) the low pressure region is above the streak and the motion in the region is a flow upward. The plane in Fig. 7(e) is located a short distance downstream of the plane in Fig. 7(d). Thus, immediately after the legs have appeared an upward motion is seen in Fig. 7(e) in the low pressure region now located above the streak, and hence forms the head of the first structure. At the other side (downstream side) of the low pressure region the motion is a downward flow, as seen in Fig. 7(f). This downward velocity at the downstream side of the head indicates that the low pressure structure is a vortex loop. Since the head is observed right after the legs, the structure is very short, which was also observed in Fig. 1.

2. Vortex formation downstream of the slot

Now that the flow above the slot and around the first structure has been studied, the flow further downstream will be investigated. The same technique is used to get an idea

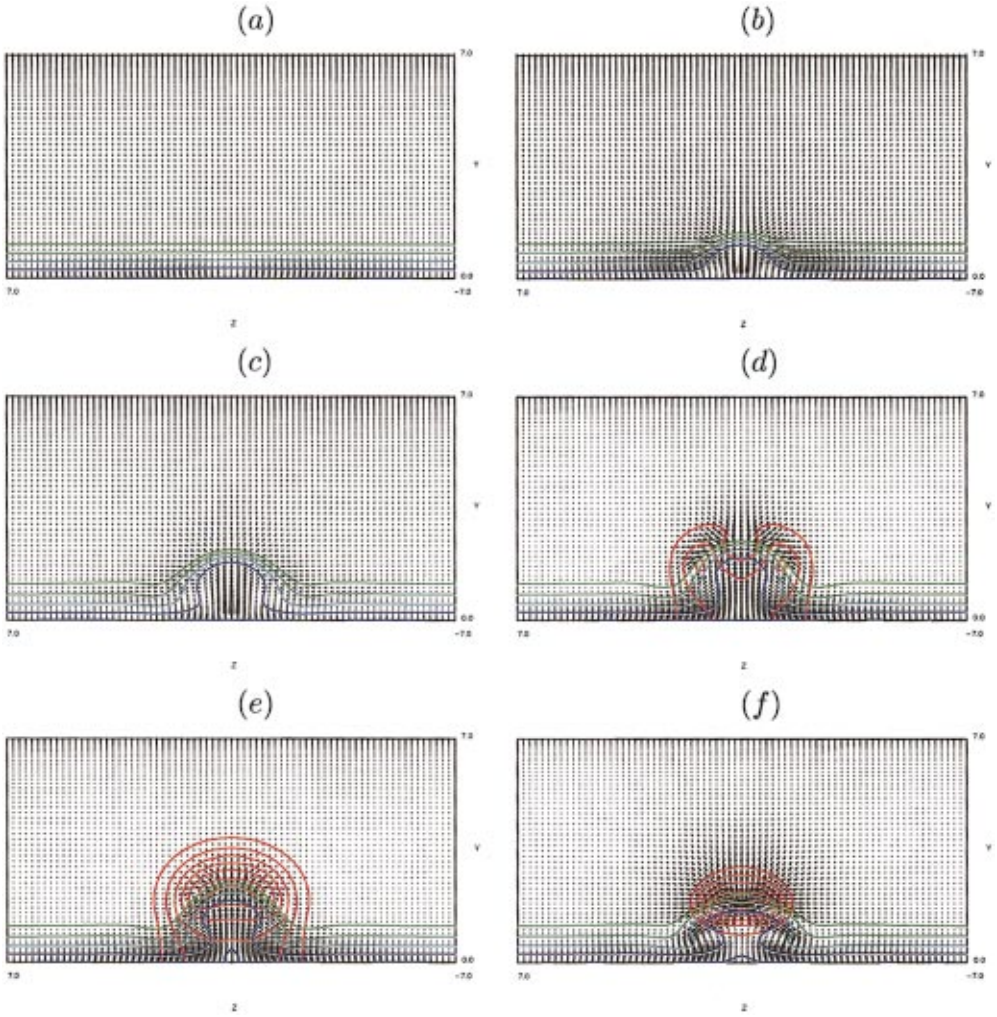

FIG. 7. (Color) Vertical planes in the spanwise (z) and normal (y) directions. Arrows represent the spanwise and normal velocity. Blue through green lines represent constant streamwise velocity from 0 to 0.5. Red lines represent constant pressure. (a) $x=30$, (b) $x=38$, (c) $x=53$, (d) $x=59$, (e) $x=60$, (f) $x=62$.

about what happens with the flow around the well developed structure indicated as number three in Fig. 1. The structure in the laminar simulation is compared with a typical structure found in the turbulent field.

In Fig. 8 vertical xy-planes are shown. In Fig. 8(a) the plane is located at the centerline ($z=0$) in the laminar field. The blue line is an iso-line of constant streamwise disturbance velocity and thus represent the low-speed streak, while the red lines are iso-lines of low pressure. The arrows indicate the normal velocity and the streamwise disturbance velocity. The streamwise disturbance velocity is calculated by subtracting the mean velocity (the mean taken in the spanwise direction) at each point. The flow is from left to right and arrows pointing to the left merely indicate low speed compared to the mean. What is seen in Fig. 8(a) is thus the head of the pressure structure. The swirling flow around the head is the relative motion when the mean streamwise velocity is subtracted. Contour levels are -0.08 for the streamwise velocity fluctuations and from -0.05 to -0.01 for the pressure.

In Fig. 8(b) a structure from the turbulent simulation is shown. The horseshoe vortex was identified with a pressure plot as in Fig. 6. The structure is representative for a turbulent structure since many can be identified in the same instantaneous pressure field. The specific structure shown in Figs. 8(b) and 9(b) is located approximately in the middle of the computational domain ($x=200$, $z=1$), and is similar to the one in the upper right corner in Fig. 6. Then a horizontal plane is cut through the center (in the spanwise direction) of the structure and its head is seen as the low pressure region in Fig. 8(b). Contour levels are -0.04 for the streamwise velocity fluctuations and from -0.02 to -0.01 for the pressure.

The similarities between Figs. 8(a) and 8(b) are remarkable. In both figures the center of rotation (relative to the local mean flow) is displaced from the center of low pressure. An additional, but weaker low pressure region is found below the head of both structures. The head of the turbulent structure in Fig. 8(b) is located at $y^+=135$.

In Fig. 9, vertical cross-stream ($yz-$) planes are shown. The red contours represent low pressure and blue to yellow lines are the iso-levels of streamwise velocity. The arrows consist of normal and spanwise velocity components. In Fig. 9(a) the legs of the structure in the laminar field are clearly

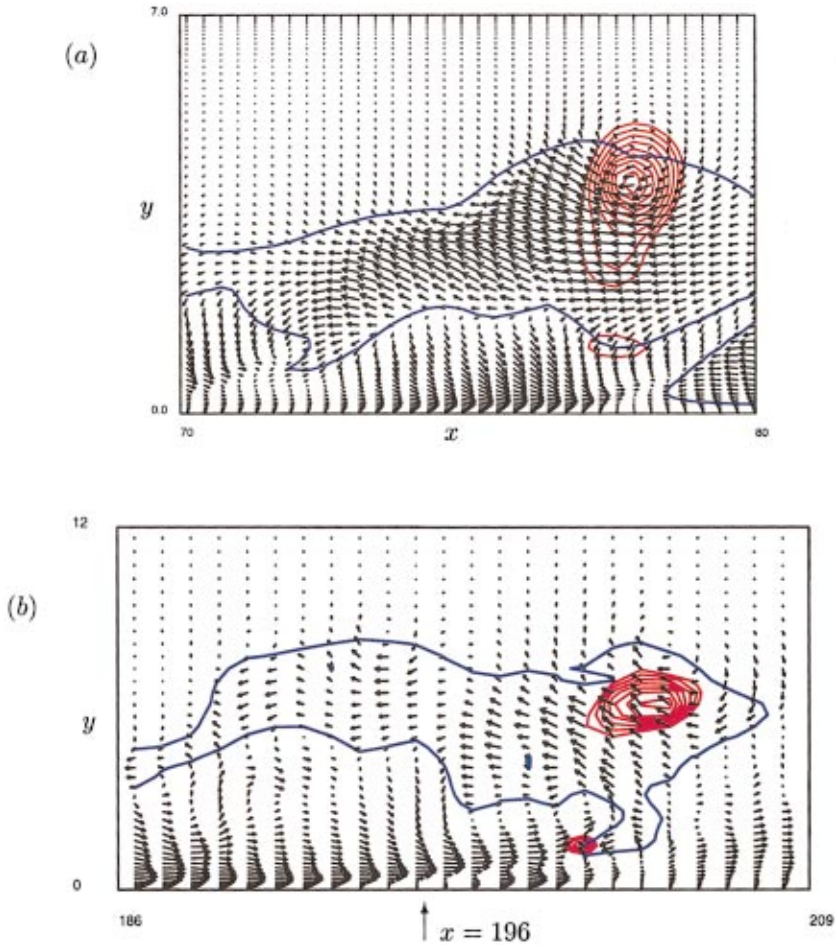

FIG. 8. (Color) Vertical planes in the streamwise (x) and normal (y) directions. Arrows represent the streamwise disturbance velocity and normal velocity components. The blue lines represent constant streamwise disturbance velocity (low-speed streak). The red color represents constant pressure (low pressure). (a) From the laminar simulation. (b) From the turbulent simulation at $z=1$.

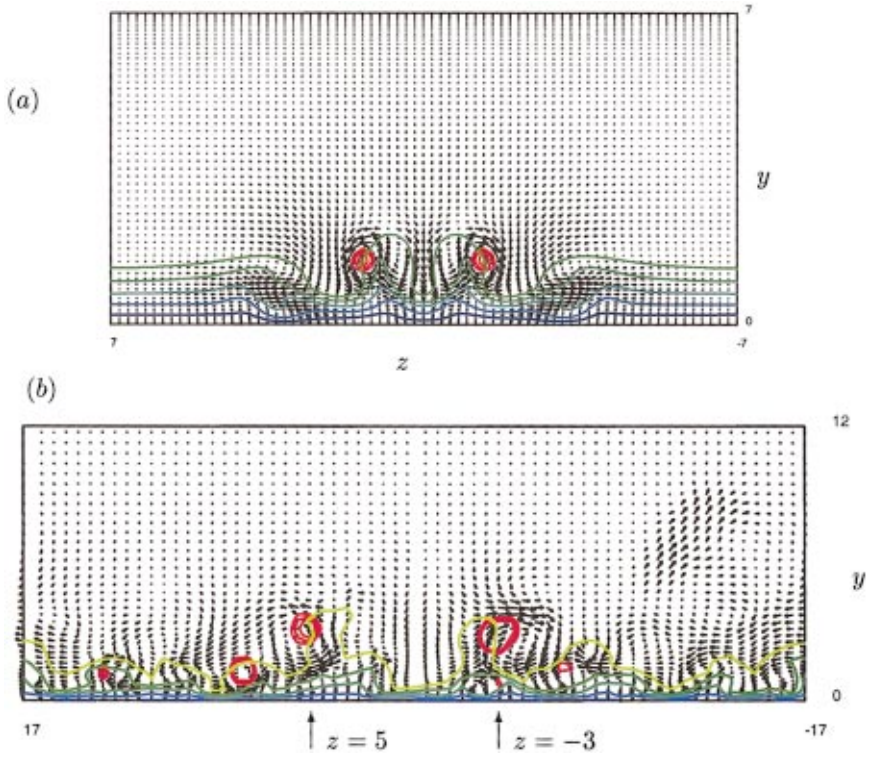

FIG. 9. (Color) Vertical planes in the spanwise (z) and normal (y) directions. Arrows represent the spanwise and normal velocity. Blue through green lines represent constant streamwise velocity. Red lines represent constant pressure. (a) From the laminar simulation. (b) From the turbulent simulation at $x=196$.

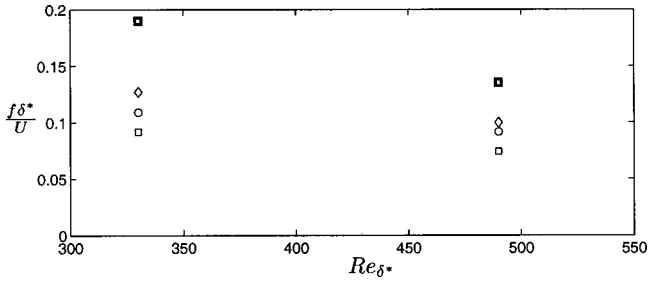

FIG. 10. Nondimensional frequency f^* of the disturbance versus $Re_{\delta*}$. Symbols correspond to different injection velocities. $Re_{V_w}=wV_w/\nu$. $Re_{V_w}=28.3$ □; $Re_{V_w}=33.6$ ○; $Re_{V_w}=38.7$ ◇. Bold symbols represent experimental data from AS.

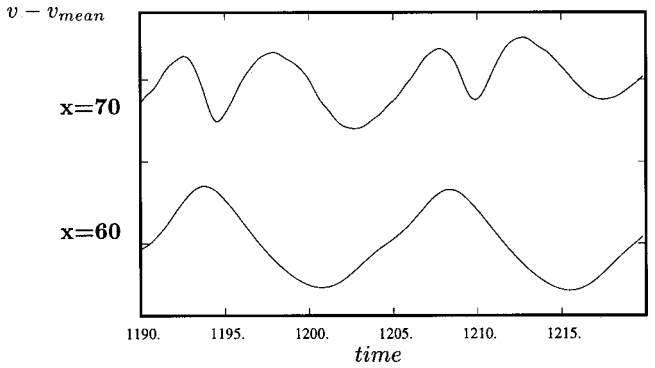

FIG. 12. Time signal of the normal velocity component at $x=60$ and $x=70$.

visible as the two low pressure regions, and the flow is circling around the low pressure. Also seen are the induced vortices further out from the centerline. These induced vortices were also observed in the experiments by AS. The plane in Fig. 9(a) is located at $x=70$, thus showing the legs belonging to the structure whose head was shown in Fig. 8(a). The blue to green contour lines represent streamwise velocity from zero to 0.5.

In Fig. 9(b), a cross-stream plane from the turbulent simulation is shown. The plane is located at $x=196$ (referring to the coordinates in Fig. 8(b), which corresponds to a distance of $x^+=184$ (wall units) upstream of the head located at $x=204$ in Fig. 8(b). The legs belonging to the horseshoe vortex whose head was observed in Fig. 8(b) are the two low pressure regions located furthest from the wall, located at $z=5$ and $z=-3$. The normal position of the legs is $y^+=70$, and they are separated with a distance $z^+=190$. The other low pressure regions close to the wall belong to streamwise vortices. The blue to yellow contour lines represent streamwise velocity from zero to 0.7. In Figs. 8(b) and 9(b) every second point in all directions is omitted for clarity.

The positions of the head and legs of the horseshoe vortex in the laminar simulation are in agreement with the experimental findings in AS. The strength of the transverse and longitudinal vortices corresponding to the head and legs were calculated in AS by assuming constant vorticity within the vortex core. However, in the present DNS we find that the vorticity varies through the core. For the vortical structures visualized by low-pressure in Figs. 8(a) and 9(a), the vorticity lines (spanwise and streamwise, respectively) formed the same pattern as the corresponding pressure contours. The vorticity ranged from -1 to -0.5 in the transverse vortex and from ± 1.5 to 0 in the longitudal vortices.

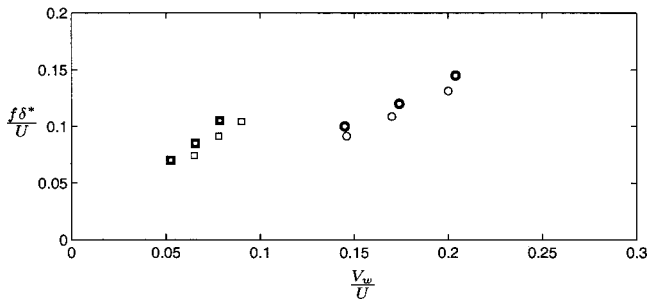

FIG. 11. Nondimensional frequency f^* of the disturbance versus V_w/U_∞. Symbols correspond to different Reynolds number. $Re_{\delta*}=490$ □; $Re_{\delta*}=330$ ○. Bold symbols represent experimental data from AS.

C. Frequency characteristics

In the experiments by AS the frequency of the roll up was measured. Their observations led to the conclusion that the frequency increased when the injection velocity or the freestream velocity was increased. They present the results as a nondimensionalized frequency ($f\delta^*/U_\infty$) as a function of slot Reynolds number ($Re_{V_w}\equiv wV_w/\nu$) and boundary layer Reynolds number ($Re_{\delta*}$) at the beginning of the slot. Here w is the width of the slot. The simulations were performed at two $Re_{\delta*}$, each with three different Re_{V_w}, for comparison with experimental results from AS. The $Re_{\delta*}$ at the beginning of the computational box were 450 and 290, corresponding to 490 and 330 at the point where the slot starts.

In the present simulations the frequency was calculated using the time-signal of the velocity from various locations in the flow. The frequency of the disturbance was observed over the full extent of the slot at a number of positions in the normal direction. When either of the two Reynolds numbers

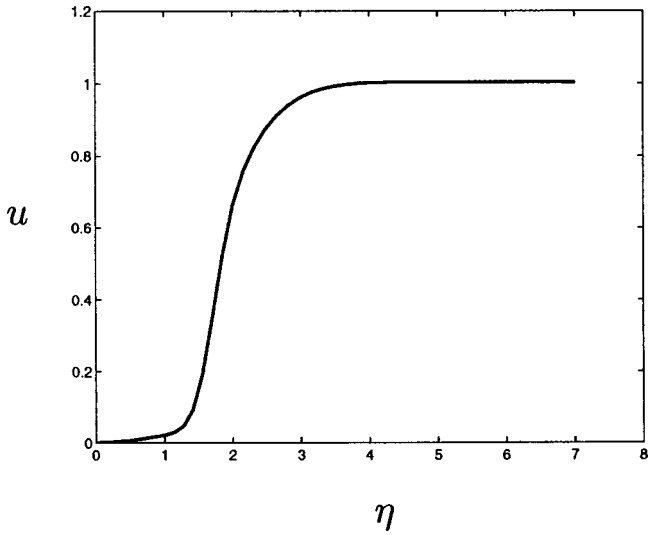

FIG. 13. Velocity profile at $x=45$.

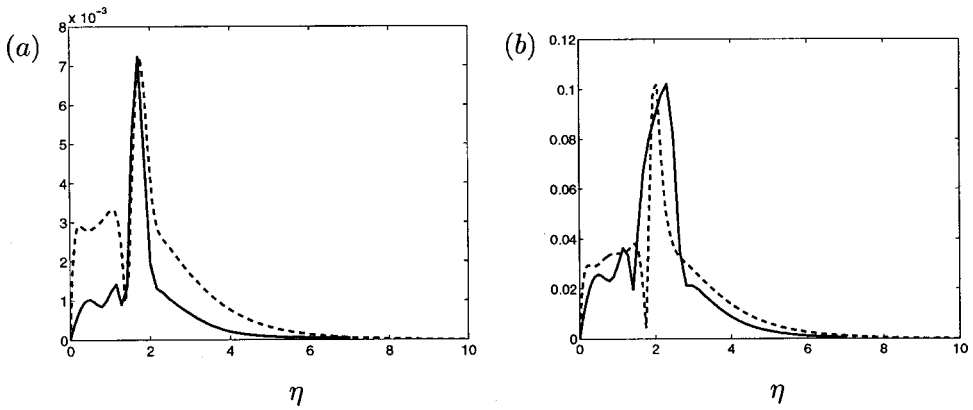

FIG. 14. Streamwise component. (a) $x=45$. (b) $x=55$. —— rms-value; - - - eigenfunction.

were changed, the frequency also changed. The frequencies for three different Re_{V_w} at two $Re_{\delta*}$ are plotted in Fig. 10, together with the results from AS (thick symbols). When the frequency is plotted as a function of the two Reynolds numbers as was done in AS, it is observed that the frequency for $Re_{V_w}=28.3$ is half of that observed by AS (Fig. 10). Also, reducing Re_{V_w} further in the simulation caused the vortex generation to cease. In the experiment by AS, $Re_{V_w}=28.3$ was the largest slot Reynolds number for which an ordered vortex generation was observed, while as low values as $Re_{V_w}=11.3$ were shown to generate vortices.

Thus, the Re_{V_w} for which vortex generation was observed in the simulations was larger than the corresponding Re_{V_w} in the experiments. For the value of $Re_{V_w}=28.3$, common to both simulation and experiment, the frequency observed in the simulation was half of that observed in the experiment. These discrepancies might be explained by the value of the blowing velocity, which is half the value in the simulation as compared to the experiment by AS. However, the slot has double width in the simulation, making the slot Reynolds number equal to the experimental value. If the blowing velocity itself, normalized by the freestream velocity, is used as the parameter in the comparison, the frequency for various blowing velocities compare well, as seen from Fig. 11. Thus, the initial guess that the slot Reynolds number in the simulation should be equal to the experimental value to obtain the same frequency is not supported by Fig. 10. Instead, it is the ratio of blowing velocity to freestream velocity that apparently is the crucial parameter in this respect, as indicated in Fig. 11. This was also suggested by AS, although they present their frequency data as in Fig. 10.

From simulation data it was observed that the frequency was doubled when going from a point above the slot to a position further downstream, as shown in Fig. 12, where the time signal of the normal component (v) of the velocity at the two downstream locations at $y=0.5$ are shown. As was shown in Sec. III B, the roll up of the structures starts right at the downstream end of the slot ($x=60$), and the frequency of the primary structures is thus the one measured at $x=60$ and not the frequency of double value which occurs further downstream at $x=70$. The doubling of the frequency is consistent with the growth of a second harmonic of the disturbance further investigated in the next section.

D. Stability analysis

In this section the laminar and turbulent simulations are treated separately.

1. The laminar case

From the observations of their experiment, AS speculate that a normal inflectional instability causes the oscillations on the low-speed streak leading to vortex roll up. Also in the experiments by Haidari and Smith[13] an unstable normal velocity profile was observed shortly before the vortex head was developed.

As described in Sec. II B, the spatial stability analysis is performed with the OS equation. The input is the Reynolds number, frequency of the disturbance, and the velocity profile. The three inputs are well defined and taken from the

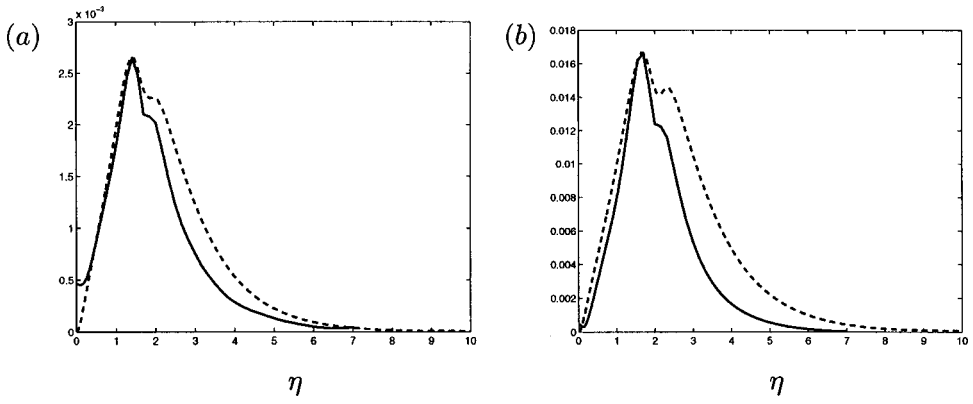

FIG. 15. Normal component. (a) $x=45$. (b) $x=55$. —— rms-value; - - - eigenfunction.

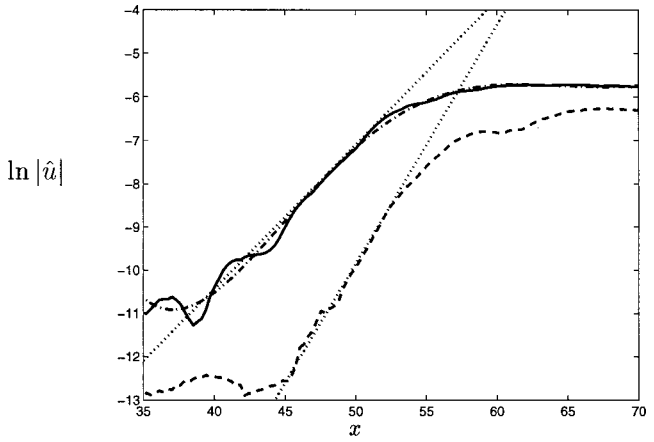

FIG. 16. Maximum of u. —— First harmonic; - - - second harmonic; ··· linear fit; —·—·—·— curve fit of first harmonic.

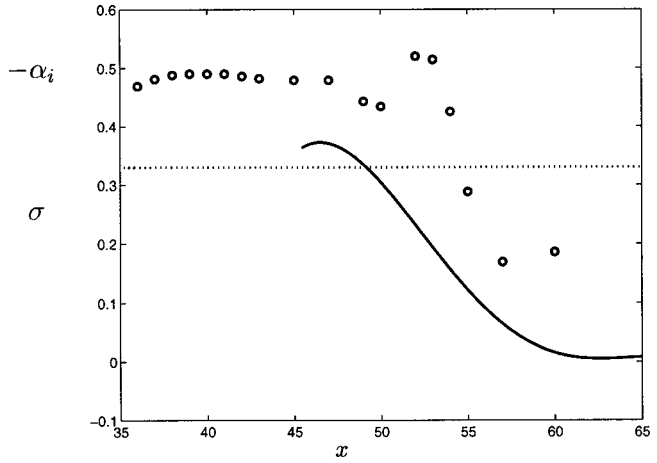

FIG. 17. ○ The growth rate from the OS analysis. —— Smoothed DNS data (curve fit). ··· Linear approximation to DNS data.

DNS. The output is the eigenfunction, which contains information of the disturbance shape, and the eigenvalue, which gives the growth rate and the streamwise wave number.

Throughout this section the laminar simulation with $Re_{\delta^*}=490$ at the beginning of the slot and a slot Reynolds number of $Re_{V_w}=28.3$ will be considered. In Fig. 13 the velocity profile at $x=45$ and $z=0$, corresponding to the center of the slot, is shown. The profile is highly inflectional and the OS analysis will give a large value of the growth rate.

Figures 14 and 15 show the eigenfunction from the OS together with the rms-value of the velocity from DNS at positions $x=45$ and $x=55$. The eigenfunctions are calculated using the instantaneous velocity profile at the two x-positions as basic states. The rms-value from DNS is calculated over one period of the disturbance, which was $T=14.8$ (in units of δ^*/U_∞) and the corresponding frequency was $\Omega=0.425$.

The eigenfunction in the streamwise direction is shown in Figs. 14(a) and 14(b), together with the corresponding u_{rms} from the DNS. The solid line is DNS data and the dashed line is from the OS analysis. The wall normal coordinate is scaled with the boundary layer thickness. The sharp peak in the profile is due to the shear layer instability. At both x positions the shape is well predicted. The double inner peak observed in the u_{rms} profile is slightly overpredicted by the OS analysis at $x=45$ and is lacking at $x=55$.

The eigenfunction in the normal direction is shown in Figs. 15(a) and 15(b), together with the corresponding v_{rms} from the DNS. The profiles are well predicted by the linear OS analysis. However, the second, outer peak is also slightly overpredicted by the linear OS analysis. Observe that v_{rms} is not zero at the wall due to the injection through the slot.

The results shown in Figs. 14 and 15 are based on an instantaneous two-dimensional approximation of the basic state. The agreement between the calculated eigenfunctions and the rms-profiles found in the fully three-dimensional DNS is remarkable, indicating that the instability mechanism is determined mainly by the local flow conditions.

The growth rate from DNS data is calculated from the Fourier transform in time of velocity fields as a function of x. When comparing the growth rate and streamwise wave number from the OS analysis with the corresponding values from DNS data, the DNS data has to be smoothed since taking derivatives directly will give spurious oscillations.

The growth rate from the DNS data, denoted by σ, is calculated from the development in time of the maximum value of the velocity in the downstream direction. The maximum value is extracted for different frequencies from the Fourier transform in time. The transformed velocity is

$$\hat{u}(x,y,z,\omega)=\int_{-\infty}^{\infty}u(x,y,z,t)e^{-i\omega t}dt. \tag{5}$$

By taking the maximum over y and z and specifying which frequency of interest, only the x-dependency is left, $\hat{u}=\hat{u}(x)$.

In Fig. 16 the maximum of $\hat{u}$ in the first and second harmonics are shown. The maximum occurs at the centerline. By showing the logarithm of the maximum as in Fig. 16, a curve fit is possible, shown as the dash–dotted line. Also in Fig. 16 the linear approximations to both the first and second harmonics are shown as the dotted lines. The slope for the second harmonic is twice the slope for the first.

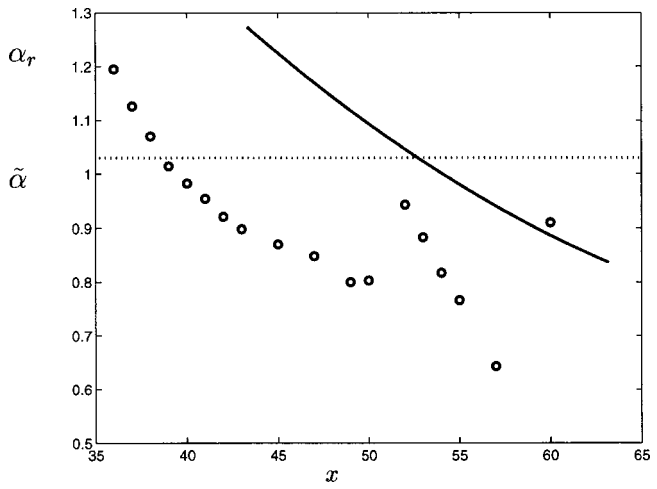

FIG. 18. ○ The streamwise wave number from OS the analysis. —— Smoothed DNS data (curve fit). ··· Linear approximation to DNS data.

Now, the growth rate is calculated from Eq. (3), which can be written as

$$\sigma = \frac{1}{|\hat{u}|}\frac{d}{dx}|\hat{u}| = \frac{d}{dx}(\ln|\hat{u}|). \tag{6}$$

The linear approximation to the maximum of $\hat{u}$ in the first harmonic (shown in Fig. 16) is used for calculating the growth rate, which becomes a constant and is shown as the dotted line in Fig. 17. By using the curve fit of $\hat{u}$ instead of the linear approximation, the growth rate becomes as the solid line shown in Fig. 17. The circles are the corresponding growth rates calculated from OS using the instantaneous velocity profiles.

The real part of the eigenvalue (α_r) from the OS analysis, is shown in Fig. 18 as circles. To calculate the corresponding α_r from DNS, which is denoted $\tilde{\alpha}$, Eq. (4) is used. This equation also involves derivatives in the downstream direction which cause spurious oscillations. To equivalently smooth the $\tilde{\alpha}$, Eq. (4) is rewritten, by noting that $\hat{u} = e^{i\Theta}$, in the form

$$\tilde{\alpha} = Re\left\{\frac{d\Theta}{dx}\right\}. \tag{7}$$

Thus, it is a matter of smoothing Θ, which is defined by

$$\Theta = -i\ln\hat{u}. \tag{8}$$

The resulting smoothed $\tilde{\alpha}$ is shown in Fig. 18. The linear approximation becomes a constant and is also shown in the figure.

Until the second harmonic has reached a substantial amplitude (see Fig. 16) the extracted results from the DNS calculation represents the true varicose secondary instability, including effects of both streamwise and spanwise variation of the base flow. Thus, the agreement between the instability analysis and DNS data presented in this section strengthen the arguments for a normal inflectional instability being the main contributor to the horseshoe vortex formation. This was also found by Park and Huerre[28] who studied streaks in curved boundary layers and showed theoretically that the sinuous mode is primarily induced by the spanwise shear, while the varicose mode is triggered by the wall-normal shear. In addition, Asai *et al.*[29] studied the response to a single low speed streak in a boundary layer excited by a time-periodic signal of either sinuous or varicose type. The growth of the sinuous mode evolved into a train of streamwise vortices and the varicose mode into horseshoe vortices.

To further show that the normal instability is of greatest interest in our case, we show the maximum normal and spanwise shear in Fig. 19. The maximum of the normal shear in Fig. 19(a) is located above the streak, and has a value of 1.3. The maximum of the spanwise shear in Fig. 19(b) is located on either side of the streak, and has a value of 0.5.

In the secondary instability calculation of Andersson *et al.*[30] the spanwise shear in a typical streak was about the same as the maximum found here. The calculated growth rate, however, was about one order of magnitude lower than the one we found from the DNS data and the presented stability calculations.

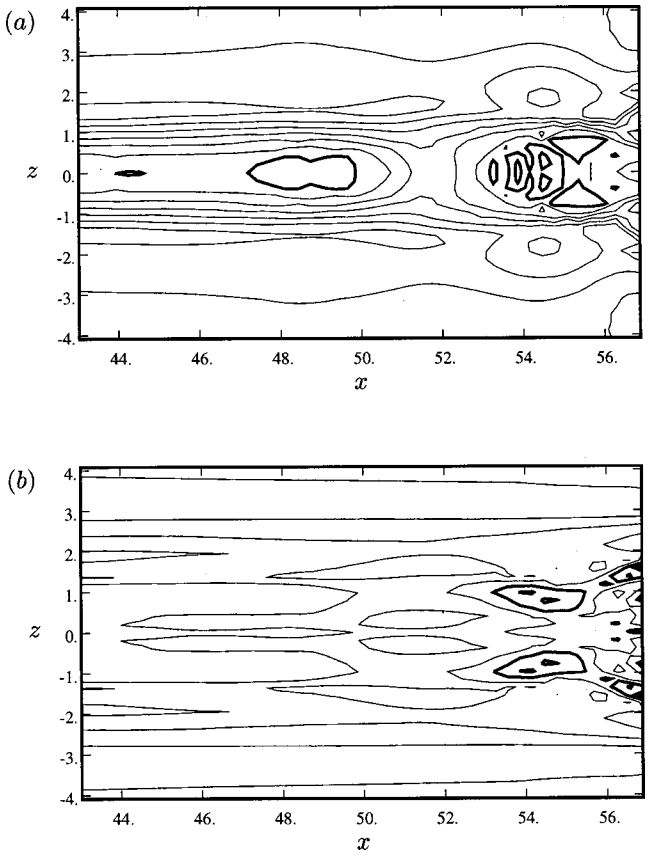

FIG. 19. Contours of maximum (over y) shear with spacing 0.1. Contours representing the largest values are indicated with thick lines. (a) Normal shear ($\max_y|\partial u/\partial y|$), maximum=1.3. (b) Spanwise shear ($\max_y|\partial u/\partial z|$), maximum=0.5.

Andersson *et al.*[30] found no varicose instability since they did not have normal velocity profiles with strong normal shear. In a parallel study (Andersson *et al.*[31]), streak profiles with strong normal shear were analyzed. In those cases the varicose mode dominated over the sinuous mode.

2. The turbulent case

So far, the detailed analysis of the low-speed streak in an otherwise laminar boundary layer has confirmed some of the results from the experiment of AS. Furthermore, a thorough analysis of the origin of the instability of the streak was made with linear stability analysis. The simulations also showed the development of more complicated structures further downstream, where the statistics resembled turbulence.

These results, together with the striking resemblance of the streak development between Figs. 6 and 1 lead to the hypothesis that, at least to some degree, the break up of streaks in a turbulent field is governed by the same mechanisms as for the isolated streak in the laminar boundary layer.

To qualitatively show that streak instabilities exist in a turbulent boundary layer that are of the same normal inflectional type as in the laminar case, the OS analysis was performed with velocity profiles from the turbulent velocity field.

When a horseshoe structure in the turbulent field has been identified, it can be followed backward in time, if ve-

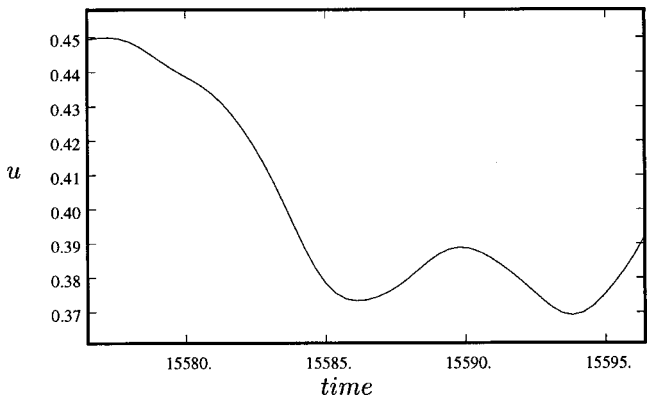

FIG. 20. Time signal of the streamwise velocity component at $x=170$, $y=0.4$, $z=-6.5$.

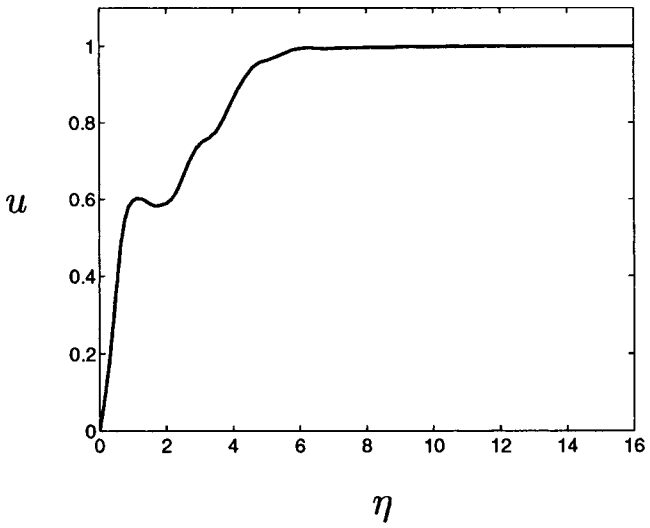

FIG. 22. Velocity profile from a turbulent boundary layer.

locity fields from earlier times are available. Since the life cycle of a structure is long (over $T=150\ \delta^*/U_\infty$), the requirement for data storage is demanding. As the structure is followed backward in time, it is found further upstream and is weaker. At some point in time and space the structure vanishes. Thus, at this point the birth of the structure can be investigated. By examining the time signal of the velocity from points just upstream of the first appearance of the structure, the frequency of the disturbance leading to the vortex formation can be determined. One example of a time signal of the streamwise velocity is shown in Fig. 20. The instability wave appears at time 15 588.

The point ($x=170$, $y=0.4$, $z=-6.5$) where the velocity signal was examined is located just upstream of the first appearance of a structure. The newly born structure is shown in Fig. 21. The figure shows the low pressure signature of the structure at the time 15 596 (referring to Fig. 20).

A velocity profile was extracted from the turbulent field at a point where the disturbance was small compared to further downstream, i.e., before roll up of the vortex. In this particular case the point was located at ($x=170$, $z=-6.5$) at the time 15 584. This profile was used together with the observed frequency in the OS equation.

To compare the DNS data with the eigenfunctions from the OS analysis, the rms-profiles were extracted by collecting statistics during a simulation over one period of the disturbance. The rms-profiles were taken from the same position as

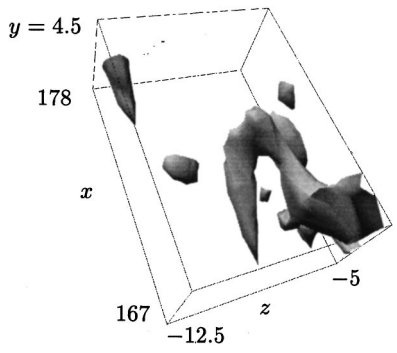

FIG. 21. Iso-surface of pressure at time 15 596. Contour level at -0.004. The height of the box shown is 4.5, corresponding to 80 in wall units.

where the frequency of the disturbance was observed for the longest period of time. This position is ($x=170$, $z=-6.5$) in the example discussed above. The time interval over which the rms-profiles were taken was 15 584–15 596.

This whole procedure was performed for three independent structures, each separated in time over 2000 (δ^*/U_∞). All three of the structures could be traced back to their point of roll up, and the analysis of the velocity profiles gave similar results.

Furthermore, the OS analysis showed that the resulting eigenfuctions are not sensitive to changes in Re_{δ^*} and frequency (ω). The independence of Reynolds number is explained by the inviscid nature of the inflectional instability. The insensitivity on ω shows that the time scale of the disturbance is not important for the instability mechanism. This points towards an instability of a Kelvin–Helmholz character.

One example of the velocity profile just before roll up is shown in Fig. 22. The frequency in this case was $\omega=0.78$ and the OS analysis gave a growth rate of $-\alpha_i=0.024$. The eigenfunctions from the OS analysis were then compared to rms-values taken over one period of the disturbance. The results from this analysis are shown in Figs. 23(a) and 23(b). In the streamwise component [Fig. 23(a)], the double peak is predicted by the linear analysis, even though the outer peak is located further out in the u_{rms} profile. In the normal component [Fig. 23(b)], the inner peak is located slightly closer to the wall in the predicted profile. Also a tendency to a second peak is seen, though the v_{rms} profile has a much stronger peak.

Although we have only investigated three randomly picked events, the results are promising and a larger investigation with an objective method for detecting structures, followed by tracing them back in time to their point of origin and the associated inflectional velocity profile, could provide statistical evidence of the horseshoe vortex formation. This is, however, beyond the scope of the present investigation.

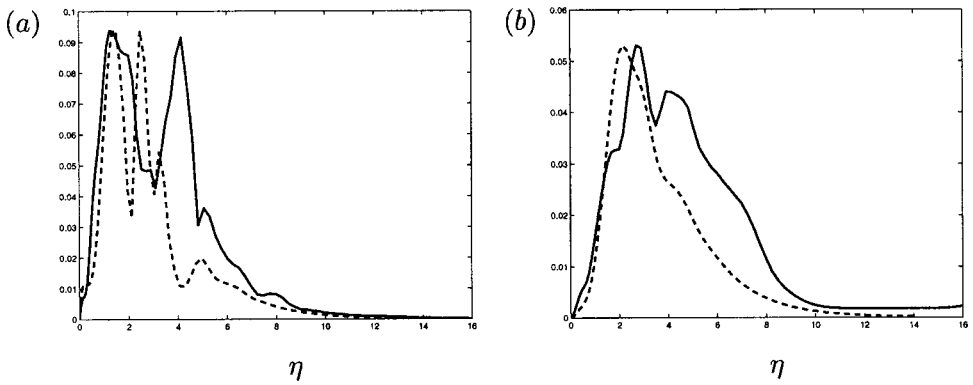

FIG. 23. (a) Streamwise component. (b) Normal component. —— rms-value of velocity. - - - Eigenfunction from the OS equation.

IV. DISCUSSION AND CONCLUSIONS

A DNS of a laminar boundary layer disturbed by a continuous blowing through a slot in the wall has been performed. The objectives were to reproduce and further investigate the results reported from the experiments of Acarlar and Smith.[12] The blowing of fluid from the slot creates a low-speed streak which exhibits a disturbance wave growing downstream. It was argued that this secondary disturbance originated from a normal inflectional instability in the streamwise velocity profile. An analysis using the Orr–Sommerfeld equations gave qualitative agreement in the growth rate and streamwise wave number with the corresponding values extracted from the DNS velocity fields. The nonlinear effects gave rise to higher harmonics at the end of the slot where the first low-pressure structure was found. The structure consist of a vortex loop that evolves downstream to form a horseshoe vortex. After the horseshoe vortex breaks down the low-speed streak persist together with additional streaks formed by the horseshoe vortex. Further downstream more complicated structures appear and the streak spacing is 100 in wall units.

The frequency of the vortex generation was shown to scale with the ratio between the blowing velocity and freestream velocity. Good agreement with the experimental data was obtained.

Also a DNS of a zero pressure gradient turbulent boundary layer was performed, and horseshoe vortices were observed using low-pressure identification. The similarities between structures in the turbulent field and the ones originating from the low-speed streak in the laminar simulation were presented. The origins of the horseshoe vortices in the turbulent boundary layer were investigated by tracing their evolution backwards in time, and the results suggested that it was related to an inflectional instability of the streaks. This is similar to the investigations of Johansson *et al.*[32] which traced the evolution of typical structures associated with the VISA events in low Reynolds number channel flow. Their investigation did not contain any stability calculations and can therefore not be directly compared to ours.

In addition, the results from our turbulent boundary layer simulation is in general agreement with the investigation of Adrian *et al.*,[14] which shows that the low-speed streak in turbulence may be spawned by horseshoe vortices. However, in the numerical experiments of turbulence where the outer part, and hence the hairpins, has been removed, the streak prevails. See, e.g., the work by Jimenez and Moin[8] and Hamilton *et al.*[9] The turbulence cycle is then dominated by the sinuous instability, which is not surprising since the varicose mode is related to hairpins which are suppressed by the geometrical constrains.

Adrian *et al.*[14] also propose a cause for the formation of the vortices themselves. They write that ''[hairpin] packets originate at the wall from a disturbance whose character is not specified except that it creates a pool of low momentum at the wall, i.e., a Q2 event from another hairpin, a bump, a puff of low momentum through the wall, a random pressure fluctuation, or a culmination of flow induced by surrounding events such as wall-tangent flows that converge to a stagnation point and thence erupt upwards.'' Our findings support this idea in the sense that the streak consists of low momentum and the varicose instability follows as a consequence.

The inflectional instability considered in the present work is of a different type from those investigated in Waleffe,[10] Kawahara *et al.*[23] and Schoppa and Hussain,[6] who model the turbulent velocity profile as a mean flow with the streaky structure deforming the profile, rather than the instantaneous profile considered here. They showed that it is the sinuous mode which is unstable. Furthermore, it has been shown in the secondary instability calculations by Andersson *et al.*,[30] that the growth rate of the sinuous mode scales with the spanwise derivative of the mean flow, just as in the model of Waleffe. Thus it is reasonable to assume that the sinuous instability depends primarily on the appearance of the spanwise inflection. Reddy *et al.*[33] further showed that the sinuous instability is inhibited by the appearance of normal shear.

We show in this work, as it has been implied in others (e.g., Robinson,[18] Asai *et al.*[29]), that the appearance of an unstable normal velocity profile (in many cases associated with a normal inflection point) is a precursor to the appearance of horseshoe vortices. In terms of a streak instability, Bottaro and Klingmann[34] among others, have shown that this is related to the varicose mode. Thus the sinuous streak instability is correlated with a basic state with a spanwise inflection and the varicose mode with a basic state with a normal inflection, as has also been shown by Park and Huerre.[28]

It is reasonable to assume that both types of streak instabilities are of importance in a turbulent boundary layer; the sinuous type for the regeneration of near-wall turbulence, as

shown by Jimenez and Moin[8] and Hamilton *et al.*,[9] and the varicose type for the production of horseshoe vortices populating the region away from the wall (see, e.g., Robinson,[18] Acarlar and Smith,[12] Haidari and Smith,[13] and Adrian *et al.*[14]).

[1]S. K. Robinson, ''Coherent motions in the turbulent boundary layer,'' Annu. Rev. Fluid Mech. **23**, 601 (1991).
[2]B. A. Singer and R. D. Joslin, ''Metamorphosis of a hairpin vortex into a young turbulent spot,'' Phys. Fluids **6**, 3724 (1994).
[3]M. S. Chong, J. Soria, A. E. Perry, J. Chacin, B. J. Cantwell, and Y. Na, ''Turbulence structures of wall-bounded shear flows found using dns data,'' J. Fluid Mech. **357**, 225 (1998).
[4]J. Zhou, R. J. Adrian, S. Balachandar, and T. M. Kendall, ''Mechanisms for generating coherent packets of hairpin vortices in channel flow,'' J. Fluid Mech. **387**, 353 (1999).
[5]J. Jeong and F. Hussain, ''Coherent structures near the wall in a turbulent channel flow,'' J. Fluid Mech. **332**, 185 (1997).
[6]W. Schoppa and F. Hussain, ''Genesis and dynamics of coherent structures in near-wall turbulence: A new look,'' *Self-Sustaining Mechanisms of Wall Turbulence*, edited by R. L. Panton (Computational Mechanics, Southampton, 1997).
[7]J. Kim, P. Moin, and R. Moser, ''Turbulence statistics in fully developed channel flow,'' J. Fluid Mech. **177**, 133 (1987).
[8]J. Jimenez and P. Moin, ''The minimal flow unit in near-wall turbulence,'' J. Fluid Mech. **225**, 213 (1991).
[9]J. H. Hamilton, J. Kim, and F. Waleffe, ''Regeneration of near-wall turbulence structures,'' J. Fluid Mech. **287**, 317 (1995).
[10]F. Waleffe, ''On a self-sustaining process in shear flows,'' Phys. Fluids **9**, 883 (1997).
[11]J. Jimenez and A. Pinelli, ''The autonomous cycle of near-wall turbulence,'' J. Fluid Mech. **389**, 335 (1999).
[12]M. S. Acarlar and C. R. Smith, ''A study of hairpin vortices in a laminar boundary layer. Part 2. Hairpin vortices generated by fluid injection,'' J. Fluid Mech. **175**, 43 (1987).
[13]A. H. Haidari and C. R. Smith, ''The generation and regeneration of single hairpin vortices,'' J. Fluid Mech. **277**, 135 (1994).
[14]R. J. Adrian, C. D. Meinhart, and C. D. Tomkins, ''Vortex organization in the outer region of the turbulent boundary layer,'' J. Fluid Mech. **422**, 1 (2000).
[15]K. T. Christensen and R. J. Adrian, ''Statistical evidence of hairpin vortex packets in wall turbulence,'' J. Fluid Mech. **431**, 433 (2001).
[16]A. E. Perry, I. Marušić, and J. D. Li, ''Wall turbulence closure based on classical similarity laws and the attached eddy hypothesis,'' Phys. Fluids **6**, 1024 (1994).
[17]I. Marušić, ''The role of large-scale structures in wall turbulence,'' Phys. Fluids **13**, 735 (2001).
[18]S. K. Robinson, ''The kinematics of turbulent boundary layer structure,'' NASA TM 103859, 1991.
[19]B. A. Singer, ''The formation and growth of a hairpin vortex,'' in *Instability, Transition and Turbulence*, edited by M. Y. Hussaini, A. Kumar, and C. L. Street (Springer, New York, 1992), pp. 367–376.
[20]H. T. Kim, S. J. Kline, and W. C. Reynolds, ''The production of turbulence near a smooth wall in a turbulent boundary layer,'' J. Fluid Mech. **50**, 133 (1971).
[21]M. T. Landahl, ''Wave mechanics of breakdown,'' J. Fluid Mech. **56**, 775 (1972).
[22]M. T. Landahl, ''On sublayer streaks,'' J. Fluid Mech. **212**, 593 (1990).
[23]G. Kawahara, J. Jimenez, M. Uhlmann, and A. Pinelli, ''The instability of streaks in near-wall turbulence,'' Center for Turbulence Research, Annual Research Briefs 1998, pp. 155–170, 1998.
[24]W. Schoppa and F. Hussain, ''Coherent structure generation in near-wall turbulence,'' J. Fluid Mech. **453**, 57 (2002).
[25]A. Lundbladh, S. Berlin, M. Skote, C. Hildings, J. Choi, J. Kim, and D. S. Henningson, ''An efficient spectral method for simulation of incompressible flow over a flat plate,'' Technical Report TRITA-MEK 1999:11, Royal Institute of Technology, Stockholm, 1999.
[26]J. Nordström, N. Nordin, and D. S. Henningson, ''The fringe region technique and the fourier method used in the direct numerical simulation of spatially evolving viscous flows,'' SIAM J. Sci. Comput. (USA) **20**(4), 1365 (1999).
[27]M. S. Chong, A. E. Perry, and B. J. Cantwell, ''A general classification of three-dimensional flow fields,'' Phys. Fluids A **2**, 765 (1990).
[28]D. S. Park and P. Huerre, ''Primary and secondary instabilities of the asymptotic suction boundary layer on a curved plate,'' J. Fluid Mech. **283**, 249 (1995).
[29]M. Asai, M. Minagawa, and M. Nishioka, ''The instability and breakdown of a near-wall low-speed streak,'' J. Fluid Mech. **455**, 289 (2002).
[30]P. Andersson, L. Brandt, A. Bottaro, and D. S. Henningson, ''On the breakdown of boundary layer streaks,'' J. Fluid Mech. **428**, 29 (2001).
[31]P. Andersson, A. Bottaro, D. S. Henningson, and P. Luchini, ''Secondary instability of boundary layer streaks based on the shape assumption,'' Technical Report TRITA-MEK 1999:13, Royal Institute of Technology, Stockholm, 1999.
[32]A. V. Johansson, P. H. Alfredsson, and J. Kim, ''Evolution and dynamics of shear-layer structures in near-wall turbulence,'' J. Fluid Mech. **224**, 579 (1991).
[33]S. C. Reddy, P. J. Schmid, P. J. Bagget, and D. S. Henningson, ''On stability of streamwise streaks and transition thresholds in plane channel flows,'' J. Fluid Mech. **365**, 269 (1998).
[34]A. Bottaro and B. G. B. Klingmann, ''On the linear breakdown of Görtler vortices,'' Eur. J. Mech. B/Fluids **15**, 301 (1996).